

'Big Bang' tomography as a new route to atomic-resolution electron tomography

Dirk Van Dyck¹, Joerg R. Jinschek² & Fu-Rong Chen³

Until now it has not been possible to image at atomic resolution using classical electron tomographic methods¹, except when the target is a perfectly crystalline nano-object imaged along a few zone axes². The main reasons are that mechanical tilting in an electron microscope with sub-ångström precision over a very large angular range is difficult, that many real-life objects such as dielectric layers in microelectronic devices impose geometrical constraints and that many radiation-sensitive objects such as proteins limit the total electron dose. Hence, there is a need for a new tomographic scheme that is able to deduce three-dimensional information from only one or a few projections. Here we present an electron tomographic method that can be used to determine, from only one viewing direction and with sub-ångström precision, both the position of individual atoms in the plane of observation and their vertical position. The concept is based on the fact that an experimentally reconstructed exit wave^{3,4} consists of the superposition of the spherical waves that have been scattered by the individual atoms of the object. Furthermore, the phase of a Fourier component of a spherical wave increases with the distance of propagation at a known 'phase speed'. If we assume that an atom is a point-like object, the relationship between the phase and the phase speed of each Fourier component is linear, and the distance between the atom and the plane of observation can therefore be determined by linear fitting. This picture has similarities with Big Bang cosmology, in which the Universe expands from a point-like origin such that the distance of any galaxy from the origin is linearly proportional to the speed at which it moves away from the origin (Hubble expansion). The proof of concept of the method has been demonstrated experimentally for graphene with a two-layer structure and it will work optimally for similar layered materials, such as boron nitride and molybdenum disulphide.

Consider a coherent plane electron wave that interacts with a single atom. If we assume the atom to be a single point, it acts as a source for a spherical wave (Ewald sphere) that propagates to the plane of detection (the image plane), where it interferes with the spherical waves emitted by the other atoms.

Using focal series reconstruction^{3,4} or off-axis holography⁵, it is possible to reconstruct the exit wave of the object (in the future this might even be possible using phase plates⁶). The challenge is how to determine the three-dimensional position of every individual atom of the object from the exit wave. Every spherical wave can be decomposed in terms of Fourier components. In the Fresnel approximation for the spherical wave, which is valid for high-energy electrons, the phase of each Fourier component varies linearly with increasing distance from the source and is given by $\pi \lambda g^2 f$, where λ is the wavelength, g is the spatial frequency and f is the focal distance between the atom and the plane at which the exit wave is reconstructed. Thus, if we select the exit wave around the projection of a particular atom, Fourier transform the wave and plot the respective phases of the Fourier components as function of the square of the spatial frequency, we obtain a straight line. This plot is analogous with the Hubble plot^{7,8} in cosmology, which shows that the distance and recessional speed of a distant galaxy are related linearly. By linear fitting of our plot, we obtain the vertical distance from the atom to the plane of observation (the reconstructed exit wave). In our analogy, this distance is the counterpart of the time between the Big Bang^{7,8} and the present (Fig. 1).

We assume that for high-energy electrons the scattering is forward and that a single atom is a weak-phase object. This allows us to neglect multiple scattering and electron propagation inside the atom. Within the weak-phase object approximation, the electron wavefunction immediately behind the atom, that is, on the same side as the plane of observation, is then given by

$$\psi(r) = 1 + iV_{p}(r) \tag{1}$$

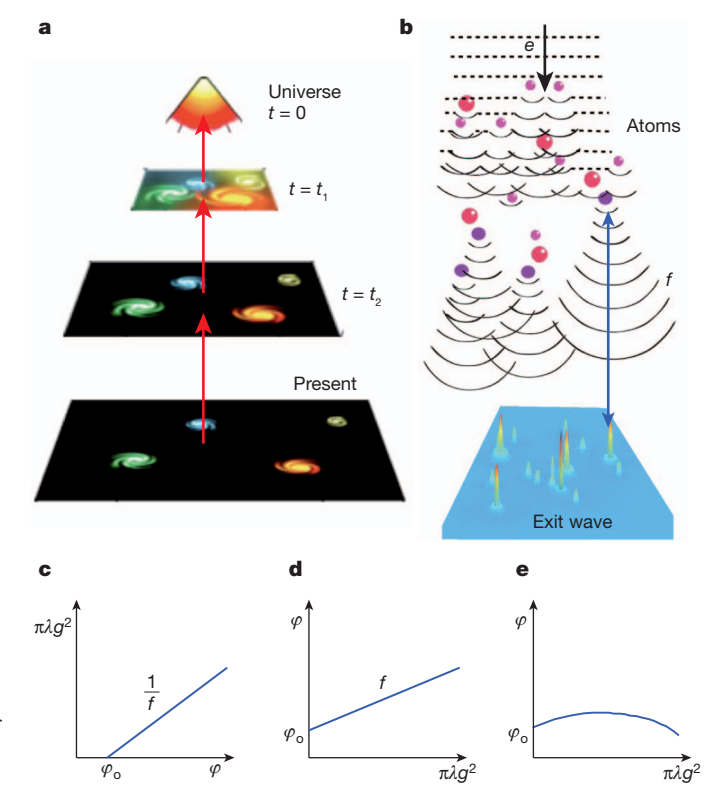


Figure 1 | Big Bang analogy. a, b, Comparison between the Big Bang (a) and the point-atom 'big bang' (b). c, Phase speed plotted against phase. The relationship between the two is the same as that expressed in cosmology by Hubble's law, which gives the linear relationship between the distance and the speed of a distant galaxy. Here the slope is the reciprocal focal distance, 1/f. Note that at the position of the atom, the phase of the atom wave does not start from zero; instead, it has a value, φ_{o} , characteristic of the atom. d, Phase plotted against phase speed, which we refer to as the Hubble plot here. The slope gives the focal distance between the emitting atom and the plane of reconstruction of the exit wave. e, Same as in d, but with a minor residual spherical aberration with $C_s = 0.3 \, \mu \mathrm{m}$ (see text).

¹University of Antwerp, Groenenborgerlaan 171, B2020 Antwerp, Belgium. ²FEI Europe, Europe NanoPort, Achtseweg Noord 5, 5651 CG Eindhoven, The Netherlands. ³National Tsing Hua University, Number 101, Section 2, Kuang-Fu Road, Hsin Chu, Taiwan 300, China.

where $V_p(r)$ is the projected electrostatic potential of the atom and r is the distance to the centre of the atom in the plane of projection.

When the electron can propagate freely behind the atom, the electron wavefunction, $\psi_e(r,z)$, at a distance z measured from the centre of the atom is given in the Fresnel approximation by convolution (\otimes) with the Fresnel propagator p(r,z), which is the parabolic approximation of the spherical wave:

$$\psi_e(r,z) = \psi(r) \otimes p(r,z) = 1 + iV_p(r) \otimes p(r,z)$$

Fourier transformation then yields

$$\psi_{\mathrm{d}}(g) = F(\psi_{\mathrm{e}}(r, z)) = \delta(g) + if^{\mathrm{el}}(g) \exp(i\pi\lambda g^2 f)$$
$$= \delta(g) + f^{\mathrm{el}}(g) \exp(i(\pi/2 + \pi\lambda g^2 f))$$

where δ is the Dirac delta function. The modulus of $\psi_{\rm d}(g)$ is the scattering factor, $f^{\rm el}(g)$, of the atom, which is the Fourier transform of the atom potential, $V_{\rm p}(r)$. Because $V_{\rm p}(r)$ is real and rotationally symmetric, $f^{\rm el}(g)$ is also real and rotationally symmetric. Thus, it does not contribute to the phase of the Fourier components. Note that the factor of i produces an offset phase shift of $\pi/2$. The difference between φ , the phase at the defocus distance f, and $\varphi_{\rm o}$, the phase at defocus 0, is more generally formulated as

$$\varphi - \varphi_0 = \pi \lambda g^2 f \tag{2}$$

We can rewrite equation (2) as

$$\pi \lambda g^2 = \frac{1}{f} (\varphi - \varphi_0) \tag{3}$$

where the factor of 1/f is equivalent to the Hubble constant, H_0 , in Hubble's law. In the weak-phase object approximation, $\varphi_0 = \pi/2$.

Note also that the expression in equation (2) is rotationally symmetric. This allows us to perform rotational averaging to reduce noise, without losing any information. Figure 1c shows a theoretical 'Hubble plot' from equation (3). Unlike in the astrophysics case, we do not have to measure the phase speed, $\pi\lambda g^2$, because we know it from theory. Hence, it is more appropriate for our purposes to switch the axes and to treat the phase speed as the independent variable (Fig. 1d). The slope in Fig. 1d is the distance between the plane of the reconstructed exit wave and the emitting atom. The projected positions of the atoms in the plane of projection can be obtained with picometre precision by comparison of the phase maxima with an ideal lattice.

In practice, an exit wave can be reconstructed from high-resolution electron microscopy images using either a weighted combination of images taken at different focus values (focal series reconstruction)^{3,4} or a hologram⁵ obtained by interference with a reference wave. However, to maximize the resolution we must not eliminate the residual aberrations but instead properly balance them. Incoherent aberrations, such as temporal and spatial incoherence9 and isotropic vibrations of the atoms and of the microscope, will mainly cause an isotropic blurring of the amplitude of an atom wave in real space, but not of the phase, and therefore affects only the precision of the atomic position measurement. Coherent aberrations such as defocus, spherical aberration and astigmatism affect only the phase in Fourier space. The effect of residual spherical aberration, which is proportional to g^4 , causes a parabolic curvature for large values of g. It turns out that our method is so sensitive that by quadratic fitting we can determine the spherical aberration constant, C_s , with a precision of more than 1 μ m. Figure 1e shows a typical example of a Hubble plot with the same focal distance as in Fig. 1d but a spherical aberration with an aberration constant of $C_{\rm s} = 0.3 \, \mu {\rm m}$ (for 80-keV electrons). As a result of this aberration, the plot deviates from a straight line. By fitting the curve with a quadratic, we can determine the residual spherical aberration constant with submicrometre precision. From the angular dependence of the atom wave in Fourier space, we can in principle also determine the non-symmetric higher-order residual aberrations, but for the moment we assume that these aberrations as well as the incoherent aberrations can be sufficiently corrected in the electron microscope.

We have successfully applied our method to the study of graphene using both simulations and experimentally reconstructed exit waves of single- and double-layer graphene observed with a $C_{\rm s}$ -corrected electron microscope at 80 keV. The graphene wave was reconstructed from a focal series of 19 high-resolution transmission electron microscope images 11. The residual aberrations of the graphene exit wave were corrected up to third order by applying a numerical phase plate and by quantitative comparison with a simulated graphene exit wave 11. Graphene is a very challenging test object for our technique because carbon atoms are very light (weak scatterers) but the distance between neighbouring atoms is very small (1.4 Å), with the result that the spherical wave of an atom is sensitive to interference from neighbours. However, the theoretical distance between the graphene layers in the double sheet is well known, and its determination therefore provides an excellent test of our method.

Figure 2 shows the phase of the exit wave of a layer of graphene that is partly overlapped by a second layer. The position analysis was carried out atom by atom, and because the theoretical positions of the atoms are known, we can estimate the statistical precision that can be obtained. There are four types of atom: those in the single layer (red); those in the lower layer that do not superpose with those in the upper layer (green); those in the two layers that superpose (brightest phase peak; blue); and those in the upper layer that do not superpose with those in the lower layer (black).

The analysis of the exit wave is done in the following steps. (i) Although the original sampling of 0.00937 nm per pixel obeys the Nyquist criterion, such that no information is lost, we need to subsample the exit wave using spline interpolation at up to 0.00268 nm per pixel (Fig. 3a) to process the data further. (ii) Figure 3b shows a subsampled area of Fig. 3a. The positions of the atoms are determined by fitting the phase peaks with Gaussian functions. The red crosses in Fig. 3b are the positions of the maxima of the fitted Gaussians. (iii) In Fig. 3c, the atom wave is isolated with a circular mark with a radius of 0.07 nm, which is half of the interatomic distance. To avoid the artefacts from the Fourier transform of a sharp circular window, we soften its edges. The background around the atom is estimated by fitting from the pixel values at the edge of the mask. (iv) A square patch of side length 0.14 nm around the isolated atom peak is selected. The modulus and phase of the isolated atom are shown colour-coded in Fig. 3d. (v) The background is calculated from the pixel values outside the mask and subtracted from the pixel values inside the mask. The modulus and phase of the isolated atom after background subtraction is shown in Fig. 3e. The value of the background wavefunction for an ideal weak-phase object is $\psi(r) = 1$ as described in equation (1).

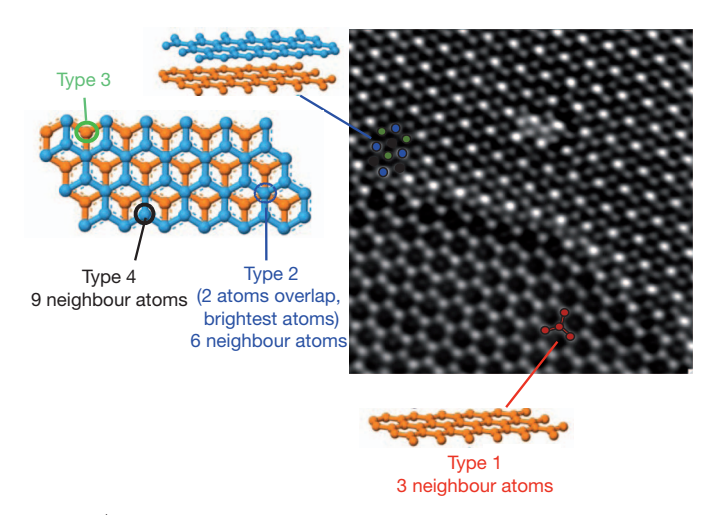


Figure 2 | Phase of the exit wave of a two-layer graphene object. Four different types of atom are distinguished: type 1 (red), type 2 (blue), type 3 (green) and type 4 (black) (see text).

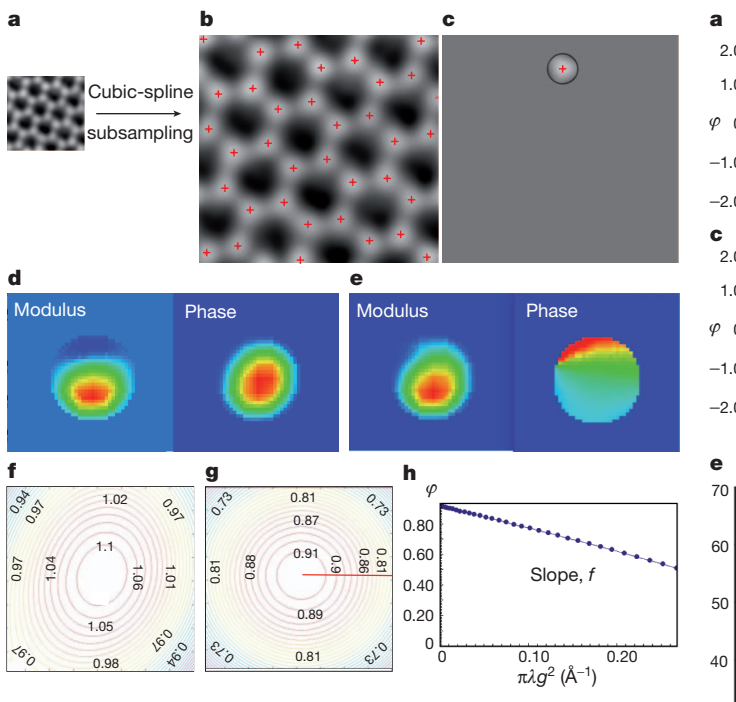


Figure 3 | Steps in the Hubble analysis. a, Subsampling of the exit wave. b, Finding the peak positions of the atom wave. c, Isolating the atom wave using a soft mask. d, Modulus and phase of the isolated atom wave. e, Modulus and phase of the isolated atom wave after background subtraction. f, Phase contour map of the Fourier transform of e. g, Phase contour map of the rotationally averaged Fourier transform. h, Hubble plot. The phase value is extracted from the red line in g.

We note that after background subtraction, the modulus of the wave should maintain the shape of V(r), whereas the phase should be a constant-phase plateau that is equal to $\pi/2$ for a weak-phase object. (vi) The background-subtracted data (Fig. 3e) is Fourier transformed. The phase contour map of the resulting Fourier transform is displayed in Fig. 3f. (vii) The Fourier transform of the wave (Fig. 3f) is rotationally averaged. The resulting phase contour map is depicted in Fig. 3g. (viii) The phase value φ (from the centre of the rotationally averaged wave) is plotted against phase speed, $\pi\lambda g^2$ (in Å⁻¹) (Fig. 3h). This is the Hubble plot described by equation (2). The depth of focus, f, that is, the distance between the atom and the plane of the exit wave, can be determined by linear regression of this plot.

By comparing these results with the 'correct' values given by the ideal lattice, using the method described above, we were able to determine the position of every atom in the plane of observation with an accuracy of about 7–10 pm as compared with the correct values given by the ideal graphene lattice (Supplementary Information and Supplementary Fig. 1). We were also able to determine the vertical position of every individual carbon atom to a precision of about 0.2 Å. Because every atom is measured independently, the standard deviation of the peak in the histogram of the defocus values, f (Fig. 4e), provides an internal measurement for the standard deviation of the whole fitting procedure.

Figure 4a–d shows the Hubble plots for four different types of atom in the graphene exit wave. In total, there are 143, 111, 115 and 100 atoms of types 1–4, respectively. The histogram of the distances of all the analysed atoms is given in Fig. 4e. The averaged f values for the four types of atom are $-0.26,\,-0.22,\,-0.18$ and $-3.5\,\text{Å}$, respectively. This corresponds to a layer separation of 3.28 Å and shows that the graphene structure has a flat bottom. This separation is close to that of ideal two-layer graphene, which is 3.35 Å (ref. 12). As shown in Fig. 4f, the flat-bottom model shows that the atoms of types 1 (red), 2 (blue) and 3 (green) are in the bottom layer and that those of type 4 (black) are in the top layer.

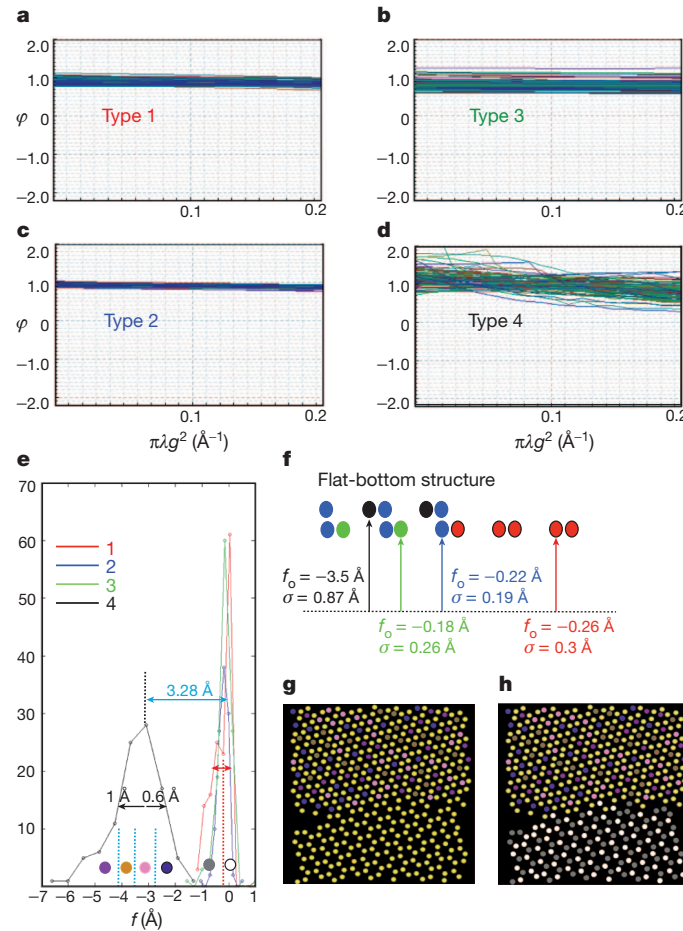


Figure 4 | **Hubble plots and histogram of the focal distance.** a–d, Hubble plots. e, Histogram of f for four different types of atom. f, The flat-bottom model. f_o , average focal distance; σ , standard deviation. g, Subtypes of atoms of type 4. h, Subtypes of atoms of type 1. Note that the sub-colours do not mean the same as in Fig. 2.

To determine the quantitative limits of precision, we analysed in detail the spread in the histograms of the vertical positions. The precisions in vertical position for atoms of types 1-4 can be derived from the standard deviation of the histogram as 0.3, 0.19, 0.26 and 0.87 Å, respectively. To analyse further the origin of the larger spread for atoms of type 4, we subdivided the histogram for these atoms into four segments, each containing the same number of atoms (Fig. 4e, blue dashed lines), colour-coded magenta, brown, pink or purple according to segment, and analysed them in real space. As shown in Fig. 4g (where atoms of types 1-3 are coloured yellow), atoms of type 4 with different focal distances are distribute randomly rather than systematically. Because we have a flat-bottom structure (Fig. 4f, where the original atom colour coding is used), each atom of type 4 has nine nearest-neighbour atoms (three in the top layer and six in the bottom layer; Fig. 2). There are, however, three near neighbours for atoms of type 1 and six for atoms of types 2 and 3. It is possible that the large spread may be due to a poor signal-to-noise ratio, which may arise from the influence of nearest-neighbour atoms, because atoms of type 4 are most highly influenced in this way.

When analysing the histogram of the atoms of the single sheet (type 1), we notice a systematic difference in vertical position between two subtypes of these atoms. In Fig. 4e, the histogram for these atoms is divided at f=-0.22 Å into two segments (red dashed line), with reference to the positions of two subpeaks in the histogram. The atoms were coloured grey or white if the associated focal values were less than or, respectively, greater than -0.22 Å. As shown in Fig. 4h, the



difference between the average vertical positions of the white and grey atoms in the histogram suggests that the single layer may have a buckled structure, but we must still consider the possibility that this effect is due to a very small asymmetric aberration. Work on this is in progress.

If we discard the few outlying atoms of type 4 (those for which f is greater than $-2.2\,\text{Å}$ or less than $-4.8\,\text{Å}$), the remainder have an average focal value of $-3.5\,\text{Å}$. The three-dimensional structure deduced from our Hubble analysis of the experimental graphene exit wave can then be formed by distinguishing the outlier atoms from the rest. Normal and perspective views of this three-dimensional structure are shown in Supplementary Fig. 2b and Supplementary Fig. 2c, respectively (see Supplementary Information, Supplementary Fig. 2 and Supplementary Movie 1 for more detail).

Received 17 November 2011; accepted 22 March 2012.

- Midgley, P. A. & Dunin-Borkowski, R. E. Electron tomography and holography in materials science. Nature Mater. 8, 271–280 (2009).
- Van Aert, S. Batenburg, K. J., Rossell, M. D., Erni, R. & Van Tendeloo, R. Threedimensional atomic imaging of crystalline nanoparticles. *Nature* 470, 374–377 (2011).
- Coene, W., Thust, A., Van Dyck, D. & Op de Beeck, M. Maximum-likelihood method for focus-variation image reconstruction in high resolution transmission electron microscopy. *Ultramicroscopy* 64, 109–135 (1996).
- Hsieh, W. K., Chen, F. R., Kai, J. J. & Kirkland, A. I. Resolution extension and exit wave reconstruction in complex HREM. *Ultramicroscopy* 98, 99–114 (2004).
- Lehmann, M. & Lichte, H. Tutorial on off-axis electron holography. *Microsc. Microanal.* 8, 447–466 (2002).

- Van Dyck, D. Wave reconstruction in TEM using a variable phase plate. Ultramicroscopy 110, 571–572 (2010).
- Hubble, E. Effects of red shifts on the distribution of nebulae. Astrophys. J. 84, 517–554 (1936).
- Hubble, E. A relation between distance and radial velocity among extra-galactic nebulae. Proc. Natl Acad. Sci. USA 15, 168–173 (1929).
- Spence, J. C. H. High Resolution Electron Microscopy 3rd edn 61, 62 (Oxford Sci. Publ., 2003).
- Bals, S., Van Aert, S., Van Tendeloo, G. & Avila-Brande, D. Statistical estimation of atomic positions from exit wave reconstruction with a precision in the picometer range. *Phys. Rev. Lett.* **96**, 096106 (2006).
- Jinschek, J. R., Yucelen, E., Calderon, H. A. & Freitag, B. Quantitative atomic 3-D imaging of single/double sheet graphene structure. Carbon 49, 556–562 (2011).
- Reich, S., Maultzsch, J. & Thomsen, C. Tight-binding description of graphene. Phys. Rev. B 66, 035412 (2002).

Supplementary Information is linked to the online version of the paper at www.nature.com/nature.

Acknowledgements We acknowledge discussions with A. Wang, S. Van Aert and I. Lobato. D.V.D. acknowledges financial support from the "Research foundation - Flanders (FWO)" under project nos G.0220.05 and G.018.08. F.-R.C. would like to acknowledge the support from NSC-100-2120-M-007-005 and NSC-99-2120-M-007-008. J.R.J. thanks E. Yucelen, R. Dunin-Borkowski and Ch. Kisielowski for support, and N. Alem and A. Zettl for the gift of the graphene sample.

Author Contributions D.V.D. and F.-R.C. read and commented on the paper, and contributed equally to the work. J.R.J. provided the experimental images of graphene.

Author Information Reprints and permissions information is available at www.nature.com/reprints. The authors declare no competing financial interests. Readers are welcome to comment on the online version of this article at www.nature.com/nature. Correspondence and requests for materials should be addressed to D.V.D. (dirk.vandyck@ua.ac.be) or F.-R.C. (frchen@ess.nthu.edu.tw).

CORRECTIONS & AMENDMENTS

CORRIGENDUM

doi:10.1038/nature11422

Corrigendum: 'Big Bang' tomography as a new route to atomic-resolution electron tomography

Dirk Van Dyck, Joerg R. Jinschek & Fu-Rong Chen

Nature 486, 243-246 (2012); doi:10.1038/nature11074

In this Letter, the name of Joerg R. Jinschek (FEI Europe, Europe NanoPort, Achtseweg Noord 5, 5651 CG Eindhoven, The Netherlands) should be included in the author list. On page 244, this sentence should be deleted: "The experimental data were obtained from ref. 11.". The Author Contributions section should include the sentence: "J.R.J. provided the experimental images of graphene.". The Acknowledgements section should include the sentence: "J.R.J. thanks E. Yucelen, R. Dunin-Borkowski and Ch. Kisielowski for support, and N. Alem and A. Zettl for the gift of the graphene sample.". The PDF and HTML versions of the original paper have been corrected online.